

Article

Large-Area Ultraviolet Photodetectors Based on *p*-Type Multilayer MoS₂ Enabled by Plasma Doping

Xiao-Mei Zhang^{1,2,*} , Sian-Hong Tseng³ and Ming-Yen Lu³¹ Department of Mechanical Engineering, Tokyo Institute of Technology, Tokyo 1528550, Japan² Department of Chemical Science and Engineering, Tokyo Institute of Technology, Tokyo 1528550, Japan³ Department of Materials Science and Engineering, National Tsing Hua University, Hsinchu 30013, Taiwan; kuroko7539510@gmail.com (S.-H.T.); mylu@mx.nthu.edu.tw (M.-Y.L.)

* Correspondence: zhang.x.as@m.titech.ac.jp

Received: 22 January 2019; Accepted: 12 March 2019; Published: 15 March 2019



Featured Application: Regarding the serious impact of UV radiation on human health, environment monitoring, and biological analysis, the demonstrated large-area *p*-type multilayer MoS₂ photodetectors exhibit great practical application for real-time UV photodetection.

Abstract: Two-dimensional (2D) MoS₂ has recently become of interest for applications in broad range photodetection due to their tunable bandgap. In order to develop 2D MoS₂ photodetectors with ultrafast response and high responsivity, up-scalable techniques for realizing controlled *p*-type doping in MoS₂ is necessary. In this paper, we demonstrate a *p*-type multilayer MoS₂ photodetector with selective-area doping using CHF₃ plasma treatment. Microscopic and spectroscopic characterization techniques, including atomic force microscopy (AFM) and X-ray photoelectron spectroscopy (XPS), are used to investigate the morphological and electrical modification of the *p*-type doped MoS₂ surface after CHF₃ plasma treatment. Back-gated *p*-type MoS₂ field-effect transistors (FETs) are fabricated with an on/off current ratio in the order of 10³ and a field-effect mobility of 65.2 cm²V⁻¹s⁻¹. They exhibit gate-modulated ultraviolet photodetection with a rapid response time of 37 ms. This study provides a promising approach for the development of mild plasma-doped MoS₂ as a 2D material in post-silicon electronic and optoelectronic device applications.

Keywords: two-dimensional; photodetection; *p*-type doping; plasma; multilayers

1. Introduction

Two-dimensional (2D) transition metal dichalcogenides (TMDCs), such as MoS₂, have attracted considerable attention owing to the unique optical and electronic properties related to its 2D ultrathin atomic layer structure [1]. MoS₂ is becoming prevalent in post-silicon digital electronics and in highly efficient optoelectronics due to its extremely low thickness and its tunable band gap ($E_g = 1\text{--}2$ eV) [2,3]. Sparsely-layered MoS₂ displays light absorbing and luminescence capabilities, enabling photodetector operation [1,3]. Several efforts have been made to further develop 2D TMDC photodetectors with ultrafast response and high responsivity [4], owing to the longer lifetime of their photo-generated carriers and higher photosensitivity than traditional semiconductors [5–7]. However, 2D TMDC photodetectors fabricated with transferred van der Waals heterostructures or chemical vapor deposition-grown hybrids are typically characterized with low responsivity. This is due to the lack of a photo-gain mechanism or by resilient photoconductivity in the heterojunction structure [8]. In order to realize MoS₂-based complementary electronic circuits and optoelectronic devices, it is necessary for there to be a development of up-scalable techniques to achieve controlled doping of MoS₂.

Recently, field-effect transistors (FETs) fabricated with MoS₂ thin films have exhibited an excellent on/off current ratio (10⁶–10⁸) with a high carrier mobility of around 200 cm² V⁻¹ s⁻¹, making them suitable for next-generation transistors [9]. For low-power, high-performance complementary logic applications, both *p*- and *n*-type MoS₂ FETs (NFETs and PFETs) must be developed. NFETs with an electron accumulation channel can be obtained using unintentionally doped *n*-type MoS₂. However, the fabrication of MoS₂ FETs with complementary *p*-type characteristics is challenging due to the significant difficulty of injecting holes into its inversion channel [10]. One approach is to use unconventional contacts resulting in a low Schottky barrier height for hole injection in MoS₂ PFETs. For example, MoO_x (2 < x < 3) contacts have been shown to be effective for hole injection into pristine MoS₂ [11]. A proper interface between MoO_x and MoS₂ layers is necessary for efficient hole injection. Alternatively, several *p*-type doping approaches for MoS₂ have been established. Examples initiated doping by incorporating substitutional niobium, Nb, atoms during chemical vapor deposition (CVD) growth and chemical doping with AuCl₃ [12–14]. However, substitutional doping during CVD growth is lacking in area selectivity and the adoption of AuCl₃ would be hampered by the risk of Au contamination. Plasma treatments with different species (including CF₄, SF₆, O₂, and CHF₃) have also been found to achieve the desired property modifications of MoS₂ [15–17]. In the case of multilayer MoS₂, which is exposed to energetic F-plasma treatment, *p*-type doping of the exposed area has been shown. However, plasma treatment may cause significant etching of the MoS₂, which can directly affect the feasibility of the development of MoS₂ FETs with a thin channel region. Therefore, mild plasma treatments are essential to achieve the proper modification of MoS₂.

In this work, we demonstrated a *p*-type multilayer MoS₂ enabled by selective-area doping using CHF₃ plasma treatment. Compared with single layer MoS₂, multilayer MoS₂ can carry a higher drive current due to its lower bandgap and multiple conduction channels. Moreover, it has three times the density of states at its minimum conduction band [18]. Back-gated MoS₂ PFETs were presented with an on/off current ratio in the order of 10³ and a field-effect mobility of 65.2 cm² V⁻¹ s⁻¹. The MoS₂ PFETs photodetector exhibited ultraviolet (UV) photodetection capability with a rapid response time of 37 ms and exhibited modulation of the generated photocurrent by back-gate voltage. Microscopic and spectroscopic characterization techniques, including atomic force microscopy (AFM) and X-ray photoelectron spectroscopy (XPS), were used to investigate the morphological and electrical modification of the MoS₂ surface after CHF₃ plasma treatment. This work suggests the potential application of the mild plasma-doped *p*-type multilayer MoS₂ in UV photodetectors for environmental monitoring, human health monitoring, and biological analysis.

2. Experimental Section

The large-area growth of MoS₂ films on 300 nm thick SiO₂/Si substrate was carried out by thermal decomposition of ammonium tetrathiomolybdate, (NH₄)₂MoS₄ (Sigma-Aldrich, St. Louis, MO, USA), in a tube furnace (Home-built). A precursor solution in 3.0 wt% was prepared by dissolving 0.292 g (NH₄)₂MoS₄ in 10 mL dimethylformamide (DMF) solvent (Sigma-Aldrich, St. Louis, MO, USA). The SiO₂/Si substrates were cleaned using a standard cleanroom protocol and subsequently treated with 100 W O₂ plasma for 5 min to improve the adhesion of the precursor solution to the substrates. After the plasma treatment, the precursor solution was promptly spin-coated onto the substrates at 1000 rpm for a period of time to form the dried (NH₄)₂MoS₄ films. Afterwards, a two-step annealing process was conducted to synthesize MoS₂ films. For the first step, the temperature was set to 280 °C for 30 min in a N₂ rich environment at 1.8 Torr. This was done to transform (NH₄)₂MoS₄ into MoS₃, as shown in previous literature [19]. To further reduce MoS₃ into MoS₂, the second step of annealing was performed. For the second step, the temperature was set to 750 °C for 30 min in a reducing atmosphere consisting of 90% Ar and 10% H₂ at 1.8 Torr. Once the heating process was completed, the furnace was allowed to cool down naturally, and a large-area sample of MoS₂ films was obtained.

3. Results and Discussion

The MoS₂ films fabricated from the thermal decomposition process were uniform and continuous based on optical microscopy (3D laser microscope, VK-X250, Keyence, Osaka, Japan), as shown in Figure 1a. This demonstrates the feasibility of the large-scale growth of homogeneous MoS₂ films by thermal decomposition for practical electronic applications. The grown MoS₂ films were subjected to out-of-plane doping by CHF₃ plasma treatment using a dry-etching system (ULVAC original NLD-570). The radiofrequency power of this dry-etching system was set to 100 W and the pressure was set to 7.5 mTorr. The final thickness of the treated samples was obtained by etching for 30 s. Figure 1b shows the optical micrograph (OM) image of the selective-area MoS₂ films with and without CHF₃ plasma treatment. On the right, the untreated region exhibits a light blue color, while on the left, the plasma-treated region displays a dark blue color. Raman spectroscopy is being used widely to study 2D materials and to identify their thicknesses. Figure 1c shows the Raman spectra of the MoS₂ films in the untreated region and in the CHF₃ plasma-treated region, respectively. Figure 1c clearly shows two main Raman features which correspond to E¹_{2g} (approximately 381 cm⁻¹) and A_{1g} (approximately 406 cm⁻¹) modes [20]. The intensity of the two peaks increases with an increase in MoS₂ film thickness. The strong, sharp peaks displayed in the Raman spectrograph of the untreated region indicate a thick layer of high crystalline MoS₂ film. On the other hand, the E¹_{2g} and A_{1g} peaks of the CHF₃-treated region are weaker due to a reduction in thickness during the plasma treatment. The energy difference between the two Raman peaks can be used to identify the number of MoS₂ layers. This energy difference value was obtained in the untreated region and equated to about 25.9 cm⁻¹, indicating a bulk-like multilayer MoS₂. However, in the CHF₃-treated region, the energy difference equated to a smaller value of 23.2 cm⁻¹, indicating a lower thickness of MoS₂ film than in the untreated region. The difference in thickness between the untreated and the CHF₃ treated region was further indicated by the difference in the E¹_{2g} and A_{1g} peak intensity between these two regions.

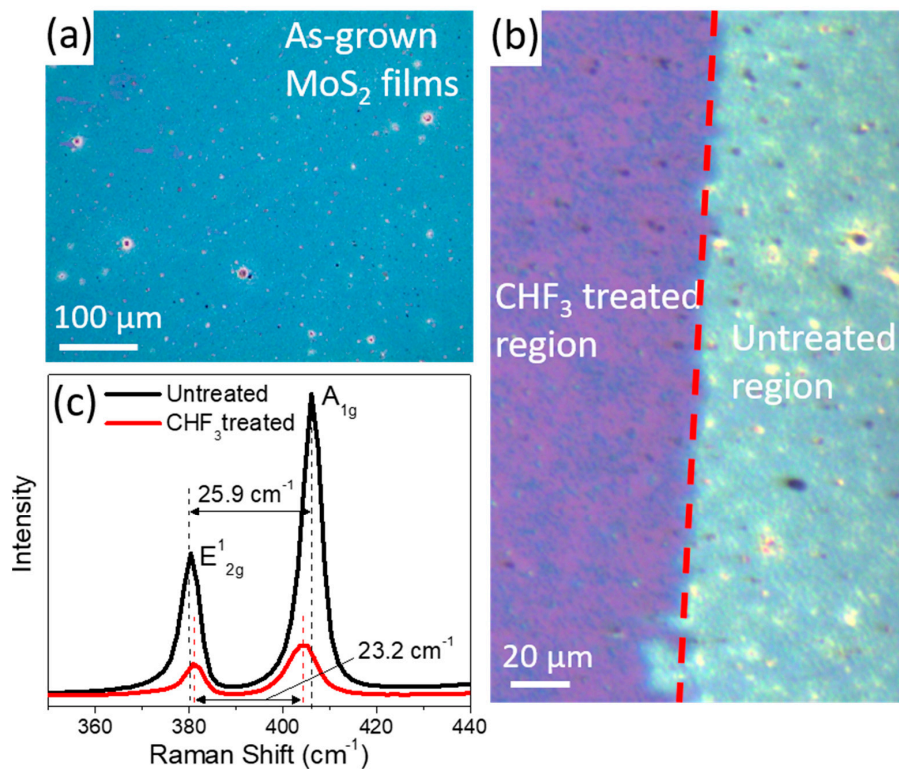


Figure 1. (a) Optical micrograph (OM) image of the as-grown MoS₂ films on the SiO₂/Si substrate. (b) OM image of the selective-area MoS₂ films with and without CHF₃ plasma treatment. (c) Raman spectra taken of the untreated and CHF₃-treated regions.

AFM (Dimension Icon, Bruker, Billerica, MA, USA) was used to examine the surface morphology and the thickness of the MoS₂ films. Figure 2a,b show the AFM image and the height profile of the as-grown MoS₂ films on the substrate, respectively. The difference in contrasts in the AFM image indicates the different heights in the image. From the height profile, the thickness of the as-grown MoS₂ was found to be about 10 nm, suggesting that there are 15 layers of MoS₂. The different contrasts in the AFM image shown in Figure 2c further indicated the thinning effect after plasma treatment. From the height profile in Figure 2d, the difference in height between the untreated and CHF₃-treated MoS₂ film was found to be approximately 4 nm. Further doping could be applied by increasing the plasma etching time; however, that would result in poor and uncontained MoS₂ films due to MoS₂ chemical modification and the formation of defects introduced by energetic ions.

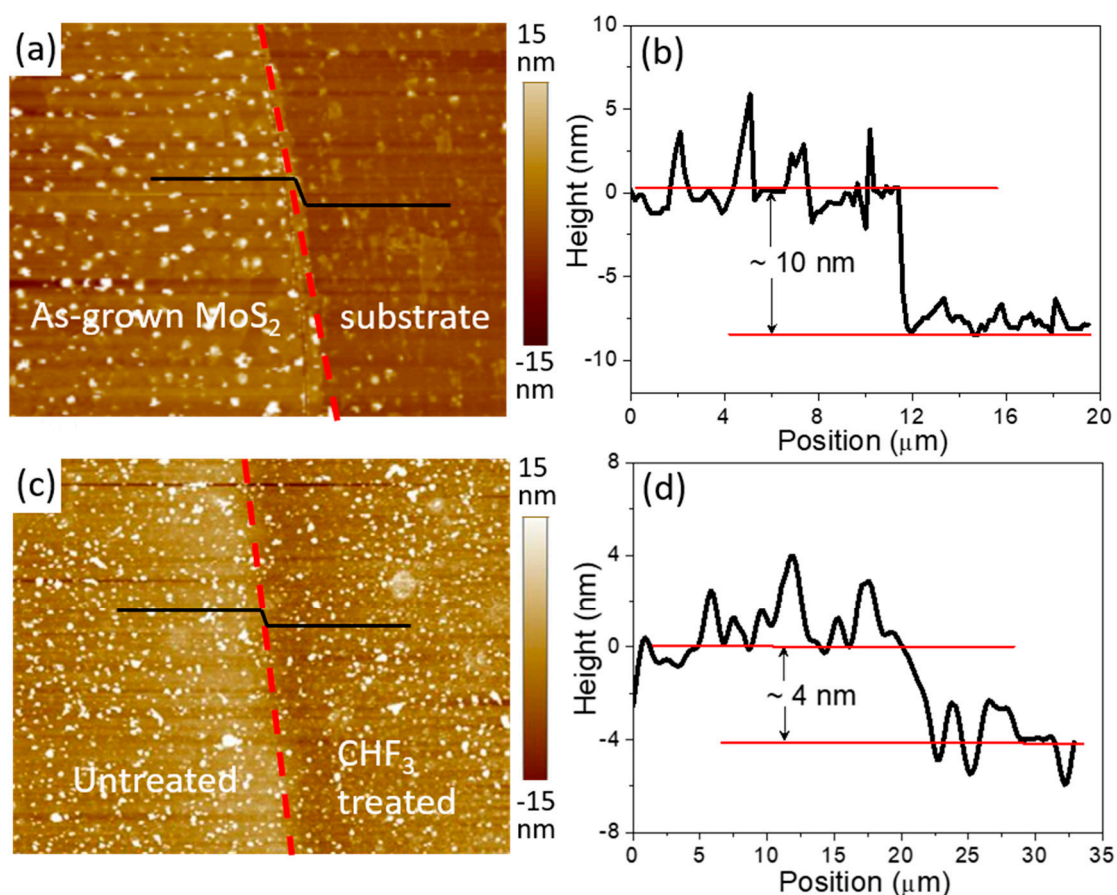


Figure 2. (a) Atomic force microscopy (AFM) height image of the as-grown MoS₂ films. (b) Line scan of the as-grown MoS₂-substrate interface. (c) AFM height image and (d) line scan across the CHF₃-treated and untreated interface of the MoS₂ film.

XPS analysis was carried out to investigate the binding energies of Mo, S, and F in the CHF₃-treated and untreated MoS₂ samples. Figure 3a,b show the detailed binding energy profiles of Mo and S for the CHF₃-treated and untreated MoS₂ samples, respectively. Two peaks at 229.8 and 232.9 eV are shown in Figure 3a. They were attributed to the doublet Mo 3d_{5/2} and Mo 3d_{3/2} of the untreated MoS₂, respectively, while the peaks of the S 2p_{3/2} and S 2p_{1/2} orbitals of the divalent sulfide ions were observed at 162.7 and 163.8 eV, respectively. These results are consistent with the reported values for untreated MoS₂ crystals [21,22]. In comparison, all relevant peaks of the CHF₃-treated sample were broader, and red-shifted by 0.57 eV. This was because of the shift in Fermi levels of the CHF₃-treated samples towards the valence band edge [23]. This red-shift of peaks indicates the proper *p*-type doping of MoS₂ films. The specific types of dopants introduced by the plasma processes were confirmed by the XPS spectra in Figure 3c. A prominent binding energy peak associated with F was observed

in CHF₃-treated samples, while the F peak was absent for untreated samples. The excess electrons were preferentially transferred from the MoS₂ layers onto F atoms with strong electronegativity when incorporating F dopants into MoS₂ layers. This surface charge transfer process suggests that F atoms are the critical dopants responsible for the *p*-type doping in MoS₂ film [24].

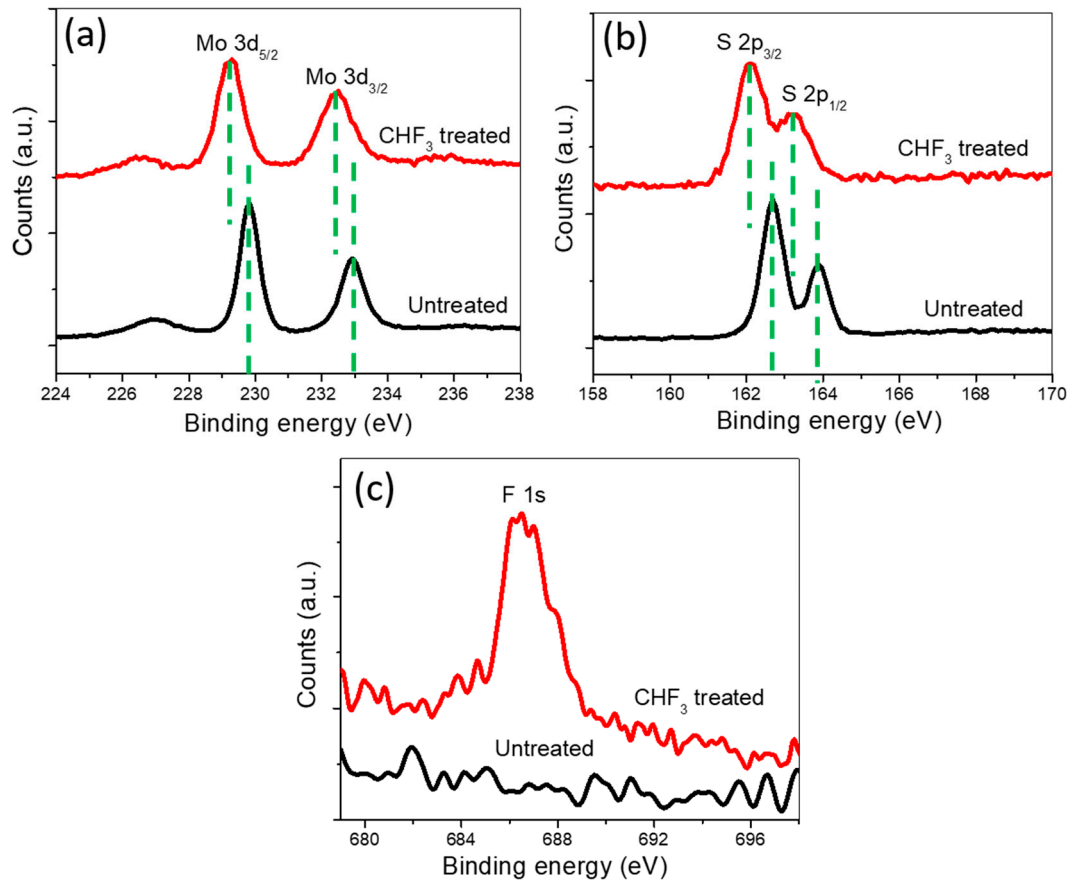


Figure 3. X-ray photoelectron spectroscopy (XPS) spectra for (a) Mo and (b) S signals before and after plasma treatment, showing a downshift of 0.57 eV in binding energy for all peaks. (c) XPS spectra for MoS₂ exhibit the presence of the F 1s peak in CHF₃ plasma-treated MoS₂.

In order to measure the electrical characteristics of the CHF₃-treated multilayer MoS₂, a back-gated FET device was fabricated as shown in the schematic illustrated in Figure 4a. Photolithography was carried out to define the exposed area of MoS₂ films for plasma treatment. After plasma treatment, 80 nm of Au was deposited as the source and as drain contacts for the FET by sputtering and was followed by lift-off. Due to the screening of the electric field in MoS₂, only the top few layers of the MoS₂ encountered a surface charge transfer process. Therefore, a thinner *n*-type MoS₂ channel at the untreated bottom layers could result in effective gate modulation and higher on/off ratios for FET applications. Figure 4b shows the output characteristics, drain current (*I*_{ds})–drain voltage (*V*_{ds}), of the MoS₂ FET under varying gate voltages (*V*_g, from 0 to −10 V). *I*_{ds} decreased with the increasing *V*_g values, indicating typical *p*-type behavior. The *I*_{ds}–*V*_{ds} characteristic of the device exhibited a low onset voltage and a linear increase of *I*_{ds} versus *V*_{ds} up to a value of *V*_{ds} approximately equal to 0.6 V, where a kink in the *I*_{ds}–*V*_{ds} curves was observed. This was followed by saturation of the *I*_{ds}–*V*_{ds} curve for *V*_{ds} greater than 0.6 V. Figure 4c represents the transfer characteristic of the back-gated MoS₂ FET at *V*_{ds} of 4 V. The back-gated MoS₂ FET showed excellent gating control capability. The field-effect mobility, μ_h , of this MoS₂ device can be estimated based on the following equation:

$$\mu_h = \frac{L}{W \times C_g \times V_{ds}} \times \frac{dI_{ds}}{dV_g}$$

where the channel length, L , is 1 mm, the channel width, W , is 1.2 mm, and the gate capacitance, C_g , is $115 \text{ aF}/\mu\text{m}^2$ for a 300 nm thick SiO_2 layer [9]. The mobility of the device was calculated to be $65.2 \text{ cm}^2 \text{ V}^{-1}\text{s}^{-1}$, which is comparable with previous results of similar back-gated FET devices [18]. However, the mobility was lower than that obtained from the top-gated FET. This difference in the mobility was due to the existence of trap states within the SiO_2 dielectric layer at the bottom gate. Moreover, the device exhibited an on/off current ratio in the order of 10^3 , and a threshold gate bias of about -5 V , whereas the MoS_2 PFET was positively biased under 4 V . This indicates that a large negative V_g (less than or equal to -5 V) is needed to tune the electron-rich layers of the bottom untreated MoS_2 layers into hole-rich layers. The energy band structures of the device under a negative gate with applied bias are shown in Figure 4d–f, where the conduction band (CB) and Fermi level (E_F) of multilayer MoS_2 were assumed to be 4.2 eV and 4.7 eV , respectively. From Figure 4d, the work function of Au was found to be about 5.1 eV . Although the E_F of the MoS_2 was shifted toward the valence band (VB) due to p -type doping, the E_F of Au still lay on the top half of the MoS_2 band. This led to a large Schottky barrier for holes along the Au/ MoS_2 interface. As shown in Figure 4e, for $V_{g(\text{th})} < V_g < 0$, holes could only pass through the barrier at a high V_{ds} due to the bending of the MoS_2 channel. As shown in Figure 4f, as the negative V_g increased, for $V_g < V_{g(\text{th})} < 0$, the hole barrier became thinner and allowed holes to penetrate through. This was consistent with the threshold gate bias (-5 V) obtained in Figure 4c. The drain current was greatly enhanced under a negative gate bias less than -5 V .

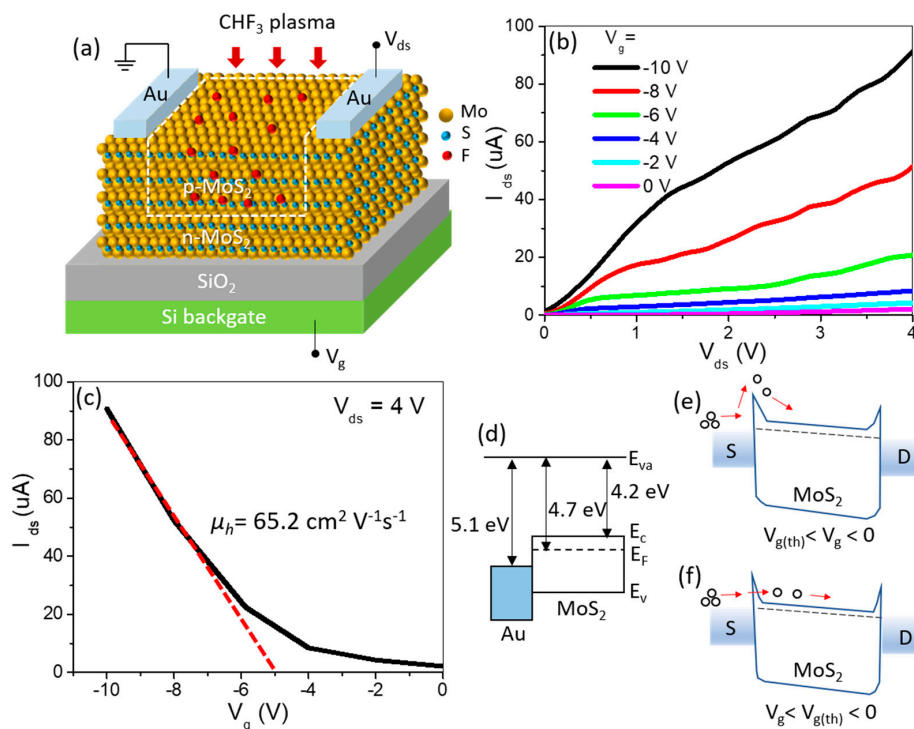


Figure 4. (a) Schematic diagram of the back-gated field-effect transistor (FET). Source and drain metal contacts are deposited on the untreated MoS_2 region. F atoms are incorporated into the upper regions of the multilayer MoS_2 . (b) I_{ds} – V_{ds} graph of the FET device at different gate bias values ranging from 0 to -10 V . (c) I_{ds} – V_g graph displaying transfer characteristic of the MoS_2 p -type FET for $V_{ds} = 4 \text{ V}$. (d–f) Band diagram of Au/ MoS_2 (d) under equilibrium condition, (e) with $V_{g(\text{th})} < V_g < 0$, and (f) with $V_g < V_{g(\text{th})} < 0$.

MoS_2 is sensitive to light illumination and is able to generate photoexcited electron–hole pairs from incident light. Figure 5a displays the photoinduced I_{ds} – V_{ds} output curves of the MoS_2 PFET excited by ultraviolet ($\lambda = 365 \text{ nm}$) light (UV lamp SLUV-8, intensity $1407 \mu\text{W}/\text{cm}^2$). The photocurrent generated at V_g from -10 V to 0 V suggests that the MoS_2 PFET can be used as a phototransistor for UV light

detection. Based on the photocurrent generated under different values of V_g , the photoresponsivity as a function of V_g is plotted in Figure 5b. The photoresponsivity increased from 0.45 A/W under zero gate voltage to 9.3 A/W under the gate voltage of 10 V, with an incident light power of 16 μ W and V_{ds} set at 4 V. The gate voltage-dependent photoresponsivity in the MoS₂ FET was due to the p -type doping of MoS₂. Under the negative V_g , E_F moved from the CB to the VB of the p -MoS₂, forming a smaller Schottky barrier between the CB of MoS₂ and the E_F of the Au electrode. This led to photogenerated charges which efficiently transferred to the external circuit and produced a large photocurrent. This photocurrent was enhanced by further increasing the negative V_g due to a thin hole Schottky barrier at the Au/MoS₂ interface. The photocurrent was also enhanced by the application of a higher positive bias V_{ds} due to the bending of the MoS₂ channel. Figure 5c shows the transfer curves of the MoS₂ device with V_{ds} equal to 4 V under UV illumination and dark conditions, respectively. Compared with dark conditions, the $V_{g(th)}$ obtained from the UV illumination had a greater absolute value. This indicates that the photoexcited holes are transferred to the electrodes due to the p -type behavior of the MoS₂, while the photoexcited electrons are trapped within the MoS₂. This is consistent with the results shown in previous literature, indicating that MoS₂ is an effective charge trapping layer [25]. The time-resolved characteristics revealed a reliable photoresponse with a stabilized photocurrent, as shown in Figure 5d. Under 365 nm illumination, the photocurrent of the MoS₂ PFET increased rapidly after exposure to UV radiation, with a rise time of 37 ms, significantly faster than those of other reported MoS₂ photodetectors [3,4,15,26], as shown in Figure 5e. This photocurrent remained nearly constant during the UV exposure (10 s) and decayed quickly during dark conditions with a decay time of approximately 39 ms. The current fully recovered after repeated cycles, which shows excellent repeatability and optical response for this MoS₂ PFET photodetector.

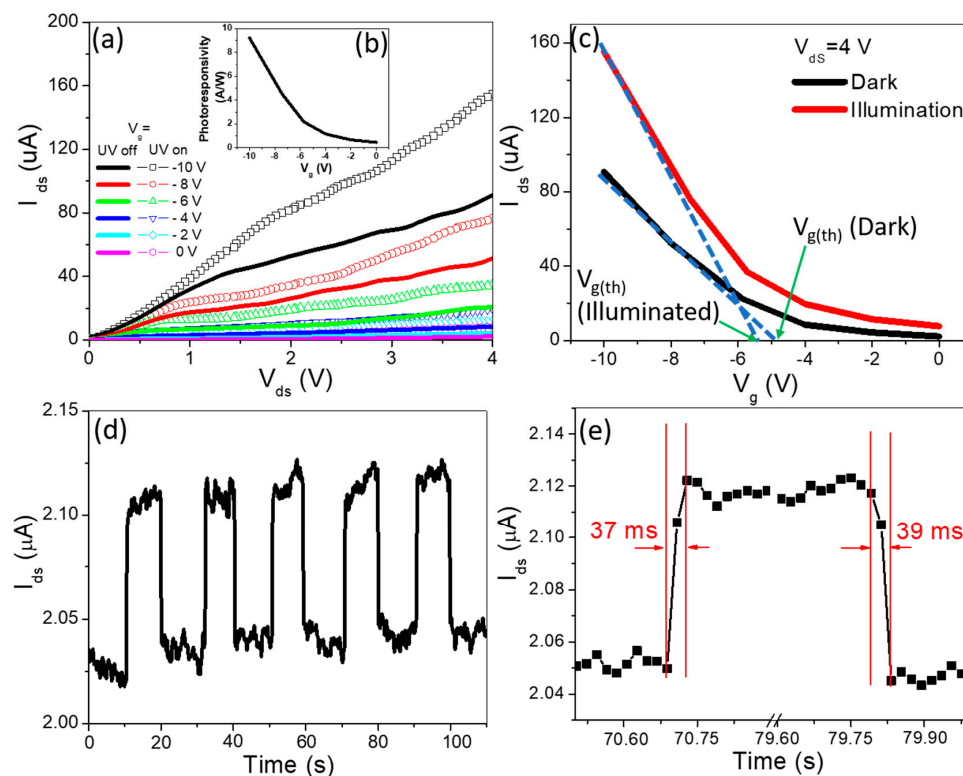


Figure 5. (a) I_{ds} – V_{ds} output curves of the MoS₂ PFET under ultraviolet ($\lambda = 365$ nm) illumination (symbols lines) and in dark conditions (solid lines) with varying gate voltages. (b) Photoresponsivity as a function of V_g at V_{ds} value of 4 V. (c) I_{ds} – V_g graph displaying transfer behavior of the MoS₂ PFET for $V_{ds} = 4$ V under dark and UV illumination. (d) Photoresponse of the p -type MoS₂ device revealing the stable and repeated changes in response to the light at on and off conditions at $V_{ds} = 6$ V. (e) Photoresponse rate of the p -type MoS₂ device.

4. Conclusions

In summary, multilayer MoS₂ photodetectors, enabled by CHF₃ plasma treatment, have been fabricated. These out-of-plane doped MoS₂ PFETs displayed an on/off current ratio in the order of 10³ and a field-effect mobility of 65.2 cm²V⁻¹s⁻¹. The MoS₂ PFETs exhibited improved UV light photodetection capability with a fast photoresponse time of 37 ms. This indicates that a vertical design could pave the way for faster MoS₂-based photodetectors. The photocurrent generation greatly depends on the back-gate voltage. This study provides a promising approach to the development of mild plasma-doped MoS₂ as a 2D material in post-silicon electronic and optoelectronic device applications.

Author Contributions: Conceptualization, X.-M.Z.; methodology, X.-M.Z. and M.-Y.L.; software, X.-M.Z.; validation, X.-M.Z.; formal analysis, X.-M.Z.; investigation, X.-M.Z.; resources, S.-H.T. and M.-Y.L.; data curation, X.-M.Z.; writing—original draft preparation, X.-M.Z.; writing—review and editing, M.-Y.L, X.-M.Z., S.-H.T.; visualization, X.-M.Z.; supervision, X.-M.Z.; project administration, X.-M.Z.; funding acquisition, X.-M.Z.

Funding: This research was funded by JST in Japan, Research and Education Consortium for the Innovation of Advanced Integrated Science (CIAiS).

Acknowledgments: We acknowledge Professor Manabu Ihara for his intellectual support and for providing access to cleanroom facilities.

Conflicts of Interest: There are no conflicts of interest to declare.

References

1. Mak, K.F.; Lee, C.; Hone, J.; Shan, J.; Heinz, T.F. Atomically thin MoS₂: A new direct-gap semiconductor. *Phys. Rev. Lett.* **2010**, *105*, 136805. [[CrossRef](#)] [[PubMed](#)]
2. Jeong, S.H.; Liu, N.; Park, H.; Hong, Y.K.; Kim, S. Temperature-dependent electrical properties of Al₂O₃-passivated multilayer MoS₂ thin-film transistors. *Appl. Sci.* **2018**, *8*, 424. [[CrossRef](#)]
3. Yin, Z.; Li, H.; Li, H.; Jiang, L.; Shi, Y.; Sun, Y.; Lu, G.; Zhang, Q.; Chen, X.; Zhang, H. Single-layer MoS₂ phototransistors. *ACS Nano* **2012**, *6*, 74–80. [[CrossRef](#)] [[PubMed](#)]
4. Lopez-Sanchez, O.; Lembke, D.; Kayci, M.; Radenovic, A.; Kis, A. Ultrasensitive photodetectors based on monolayer MoS₂. *Nat. Nanotech.* **2013**, *8*, 497–501. [[CrossRef](#)]
5. Peng, L.; Hu, L.F.; Fang, X.S. Low-dimensional nanostructure ultraviolet Photodetectors. *Adv. Mater.* **2013**, *25*, 5321. [[CrossRef](#)]
6. Zhang, X.M.; Akita, H.; Ihara, M. Epitaxial growth of silicon nanowire arrays at wafer-scale using high-speed rotating-disk CVD for improved light-trapping. *CrystEngComm* **2016**, *18*, 6153–6157. [[CrossRef](#)]
7. Torbatian, Z.; Asgari, R. Plasmonic physics of 2D crystalline materials. *Appl. Sci.* **2018**, *8*, 238. [[CrossRef](#)]
8. Li, X.; Lin, M.W.; Puzos, A.A. Persistent photoconductivity in two-dimensional Mo_{1-x}W_xSe₂-MoSe₂ van der Waals heterojunctions. *J. Mater. Res.* **2016**, *31*, 923–930. [[CrossRef](#)]
9. Radisavljevic, B.; Radenovic, A.; Brivio, J.; Giacometti, V.; Kis, A. Single-layer MoS₂ transistors. *Nat. Nanotechnol.* **2011**, *6*, 147–150. [[CrossRef](#)]
10. Giannazzo, F.; Fisichella, G.; Piazza, A.; Di Franco, S.; Greco, G.; Agnello, S.; Roccaforte, F. Effect of temperature-bias annealing on the hysteresis and subthreshold behavior of multilayer MoS₂ transistors. *Phys. Status Solidi RRL* **2016**, *10*, 797. [[CrossRef](#)]
11. Chuang, S.; Battaglia, C.; Azcatl, A.; McDonnell, S.; Kang, J.S.; Yin, X.; Tosun, M.; Kapadia, R.; Fang, H.; Wallace, R.M.; et al. MoS₂ p-type transistors and diodes enabled by high work function MoO_x contacts. *Nano Lett.* **2014**, *14*, 1337–1342. [[CrossRef](#)]
12. Das, S.; Demarteau, M.; Roelofs, A. Nb-doped single crystalline MoS₂ field effect transistor. *Appl. Phys. Lett.* **2015**, *106*, 173506. [[CrossRef](#)]
13. Liu, X.; Qu, D.; Ryu, J.; Ahmed, F.; Yang, Z.; Lee, D.; Yoo, W.J. P-type polar transition of chemically doped multilayer MoS₂ transistor. *Adv. Mater.* **2016**, *28*, 2345. [[CrossRef](#)]
14. Ko, T.-S.; Huang, C.-C.; Lin, D.-Y. Optical and transport properties of Ni-MoS₂. *Appl. Sci.* **2016**, *6*, 227. [[CrossRef](#)]

15. Xue, F.; Chen, L.; Chen, J.; Liu, J.; Wang, L.; Chen, M.; Pang, Y.; Yang, X.; Gao, G.; Zhai, J.; et al. P-type MoS₂ and n-type ZnO diode and its performance enhancement by the piezophototronic effect. *Adv. Mater.* **2016**, *28*, 3391. [[CrossRef](#)]
16. Wi, S.; Kim, H.; Chen, M.; Nam, H.; Guo, L.J.; Meyhofer, E.; Liang, X. Enhancement of photovoltaic response in multilayer MoS₂ induced by plasma doping. *ACS Nano* **2014**, *8*, 5270–5281. [[CrossRef](#)]
17. Chen, M.; Nam, H.; Wi, S.; Ji, L.; Ren, X.; Bian, L.; Lu, S.; Liang, X. Stable few-layer MoS₂ rectifying diodes formed by plasma-assisted doping. *Appl. Phys. Lett.* **2013**, *103*, 142110. [[CrossRef](#)]
18. Kim, S.; Konar, A.; Hwang, W.S.; Lee, J.H.; Lee, J.; Yang, J.; Jung, C.; Kim, H.; Yoo, J.B.; Choi, J.Y.; et al. High-mobility and low-power thin-film transistors based on multilayer MoS₂ crystals. *Nat. Commun.* **2012**, *3*, 1011. [[CrossRef](#)]
19. Lim, Y.R.; Song, W.; Han, J.K.; Lee, Y.B.; Kim, S.J.; Myung, S.; Lee, S.S.; An, K.S.; Choi, C.J.; Lim, J. Wafer-scale, homogeneous MoS₂ layers on plastic substrates for flexible visible-light photodetectors. *Adv. Mater.* **2016**, *28*, 5025. [[CrossRef](#)]
20. Ataca, C.; Topsakal, M.; Akturk, E.; Ciraci, S. A comparative study of lattice dynamics of three- and two-dimensional MoS₂. *J. Phys. Chem. C* **2011**, *115*, 16354–16361. [[CrossRef](#)]
21. Rao, C.N.R.; Nag, A. Inorganic Analogues of Graphene. *Eur. J. Inorg. Chem.* **2010**, *27*, 4244. [[CrossRef](#)]
22. Altavilla, C.; Sarno, M.; Ciambelli, P. A novel wet chemistry approach for the synthesis of hybrid 2D free-floating single or multilayer nanosheets of MS₂@oleylamine (M = Mo, W). *Chem. Mater.* **2011**, *23*, 3879–3885. [[CrossRef](#)]
23. Mahns, B.; Roth, F.; Knupfer, M. Absence of photoemission from the Fermi level in potassium intercalated picene and coronene films: Structure, polaron, or correlation physics? *J. Chem. Phys.* **2012**, *136*, 134503. [[CrossRef](#)]
24. Yue, Q.; Chang, S.; Qin, S.; Li, J. Functionalization of monolayer MoS₂ by substitutional doping: A first-principles study. *J. Phys. Lett. A* **2013**, *377*, 1362–1367. [[CrossRef](#)]
25. Zhang, E.; Wang, W.; Zhang, C.; Jin, Y.; Zhu, G.; Sun, Q.; Zhang, D.W.; Zhou, P.; Xiu, F. Tunable charge-trap memory based on few-layer MoS₂. *ACS Nano* **2015**, *9*, 612–619. [[CrossRef](#)]
26. Zhang, X.; Zhou, W.; Peng, Y.; Zhou, Y.; Zhou, F.; Yin, Y.; Tang, D. Multi-layered MoS₂ phototransistors as high performance photovoltaic cells and self-powered photodetectors. *RSC Adv.* **2015**, *5*, 45239–45248. [[CrossRef](#)]

